Journal of Power Sources 228 (2013) 1–6

Contents lists available at SciVerse ScienceDirect

Journal of Power Sources

journal homepage: www.elsevier.com/locate/jpowsour

Enhanced sinterability and electrical properties of $GdSmZr_2O_7$ by addition of nickel oxide

Zhan-Guo Liu [a,b,c], Jia-Hu Ouyang [a,*], Ke-Ning Sun [b,c], Yu Zhou [a]

[a] Institute for Advanced Ceramics, School of Materials Science and Engineering, Harbin Institute of Technology, 92 West Da-Zhi Street, Harbin 150001, China
[b] Natural Science Research Center, Academy of Fundamental and Interdisciplinary Sciences, Harbin Institute of Technology, 2 Yi-Kuang Street, Harbin 150080, China
[c] Department of Applied Chemistry, Harbin Institute of Technology, 92 West Da-Zhi Street, Harbin 150001, China

HIGHLIGHTS

- The $GdSmZr_2O_7$ ceramic exhibits a single phase of the pyrochlore-type structure.
- 1 wt.% of NiO to $GdSmZr_2O_7$ promotes sintering densification.
- 1 wt.% of NiO to $GdSmZr_2O_7$ reduces sintering temperature by about 200 K.
- Total conductivity of $GdSmZr_2O_7$ was not adversely affected by the addition of NiO.

ARTICLE INFO

Article history:
Received 22 July 2012
Received in revised form
17 November 2012
Accepted 21 November 2012
Available online 28 November 2012

Keywords:
Rare-earth zirconate
Sintering aid
Electrolyte
Electrical properties

ABSTRACT

The effect of nickel oxide addition on the sintering behavior and electrical properties of the $GdSmZr_2O_7$ ceramic has been investigated. The crystal structure, microstructure and electrical properties of the $GdSmZr_2O_7$ ceramic incorporated with or without 1 wt.% nickel oxide are characterized by the X-ray diffraction, field-emission scanning electron microscopy and electrochemical impedance spectroscopy, respectively. The $GdSmZr_2O_7$ ceramic exhibits a single phase of the pyrochlore-type structure. No chemical reaction between $GdSmZr_2O_7$ and NiO is found in the sintered samples. The grain, grain boundary, and total conductivity of the $GdSmZr_2O_7$ ceramic with or without NiO addition obey the Arrhenius relation. The addition of a small amount of NiO to the $GdSmZr_2O_7$ ceramic greatly promotes the densification process, achieving 93% of the theoretical density after sintering at 1773 K in air. This reduces the sintering temperature by about 200 K, without adversely affecting the total conductivity of the $GdSmZr_2O_7$ ceramic. The $GdSmZr_2O_7$ ceramic with 1 wt.% NiO addition is an oxide-ion conductor in the oxygen partial pressure range of 1.0×10^{-4} to 1.0 atm at all test temperature levels.

1. Introduction

In recent years, solid oxide fuel cells (SOFCs) have received much attention in scientific community due to the combined advantages such as potential long-term stability and economical competitiveness for some vehicles and stationary applications [1–3]. In the past decades, YSZ (8 mol.% yttria-stabilized zirconia)-based materials have been widely studied as the solid electrolyte material [4–6]. At the same time, the anode material is usually Ni–YSZ cermet, and the cathode material is generally strontium-substituted manganites ($La_{1-x}Sr_xMnO_3$). However, high operating temperature promotes unwanted chemical reactions at the electrolyte/cathode interface, and leads to form $La_2Zr_2O_7$ and $SrZrO_3$ resistive layers [7,8]. Both $La_2Zr_2O_7$ and $SrZrO_3$ phases result in the decrease of electrical conductivity, and the degradation on the performance of SOFCs. Therefore, lowering the operating temperature is one of the main objectives for the SOFCs development. For this purpose, the current emphasis mainly focuses on the search for other solid oxide electrolytes with a higher electrical conductivity [11–13].

Rare-earth zirconates with a general formula $A_2Zr_2O_7$ (A = lanthanide), exhibit a pyrochlore-type structure or a defect fluorite-type structure, and show the well-known ability of the crystal structure to accommodate oxygen nonstoichiometry [9]. Shinozaki et al. [10] reported that the electrical conductivity of $Sm_2Zr_2O_7$ ceramic was comparable to those of other oxide-ion conductors in the low-temperature regions. In recent years, great efforts can be found on improving the electrical conductivity $A_2Zr_2O_7$-type compounds by doping with different metallic cations

* Corresponding author. Tel./fax: +86 451 86414291.
E-mail address: ouyangjh@hit.edu.cn (J.-H. Ouyang).

0378-7753/$ – see front matter © 2012 Elsevier B.V. All rights reserved.
http://dx.doi.org/10.1016/j.jpowsour.2012.11.072

[7,11,12]. $Sm_2Zr_2O_7$ co-doped with 5 mol.% Gd and 5 mol.% Yb shows a higher electrical conductivity than undoped $Sm_2Zr_2O_7$ in the temperature range of 723–1023 K [13]. The $GdSmZr_2O_7$ ceramic had the highest electrical conductivity in the $(Gd_{1-x}Sm_x)_2Zr_2O_7$ ($0 \leq x \leq 1.0$) system from 623 to 873 K [14]. However, rare-earth zirconates including the $GdSmZr_2O_7$ ceramic have poor sinterability, and usually need high sintering temperature (over 1973 K) to obtain dense bulk materials [15–17]. NiO was reported as an effective sintering aid for some oxide electrolytes, such as YSZ and perovskite-type zirconates and cerates [18–20]. NiO is usually used in the anode material of a SOFC, and therefore the addition of a small amount of NiO to the electrolytes will not complicate the composition but could be beneficial to the sintering densification of materials.

It should be noted that the sintering condition has a critical effect on the electrical conductivity of different solid oxide electrolytes. In this work, the $GdSmZr_2O_7$ ceramic with or without 1 wt.% NiO addition was prepared by pressureless-sintering method at different sintering temperatures. The effect of 1 wt.% NiO addition on the sintering behavior and electrical properties of the $GdSmZr_2O_7$ ceramic were investigated.

2. Experimental procedure

Polycrystalline gadolinium–samarium zirconate ($GdSmZr_2O_7$) ceramic, with or without a small amount (1 wt.%) of nickel oxide addition (designated with the sample codes of GSZ and NGSZ, respectively), were prepared by a solid state reaction method. Starting materials were commercial Gd_2O_3 (Rare-Chem Hi-Tech Co., Ltd, China; purity $\geq$ 99.99%), Sm_2O_3 (Rare-Chem Hi-Tech Co., Ltd, China; purity $\geq$ 99.99%), ZrO_2 (Dongguan SG Ceramics Technology Co., Ltd, China; purity $\geq$ 99.9%), and NiO (Sinopharm Chemical Reagent Co., Ltd, China; purity $\geq$ 99.9%) powders. All ceramic powders were calcined at 1173 K for 2 h in air prior to weighing. Different starting compound powders with the desired molar ratios were weighed, and mixed by ball-milling with zirconia balls and ethanol for 24 h. The mixtures were uniaxially dry pressed at 20 MPa for 2 min in a stainless steel die, and then cold isostatically pressed at 200 MPa for 5 min. The green pellets had a diameter of 13 mm, with a thickness of about 3 mm. The disc samples were sintered in air at temperatures of 1773–1973 K for 10 h, and subsequently cooled to room temperature.

X-ray diffraction (XRD, Rigaku D/Max 2200VPC, Japan) with Cu Kα radiation was used to analyze the crystal structure of the sintered samples. X-ray tube voltage and current were set at 40 kV and 30 mA, respectively. Data were collected in the 2θ range of 10° and 70° with a scanning rate of 5° min^{-1}, while slow step-scans with a step width of 0.02° and a step time of 3 s were carried out on the diffraction peak of (622) in the 2θ range of 56–60°. The bulk density of sintered samples was determined by the usual volume and weight measurement technique. The theoretical density of sintered samples was calculated by using mixing rule according to the density and volume content of $GdSmZr_2O_7$ and NiO. The morphology of the sintered samples was observed using a field-

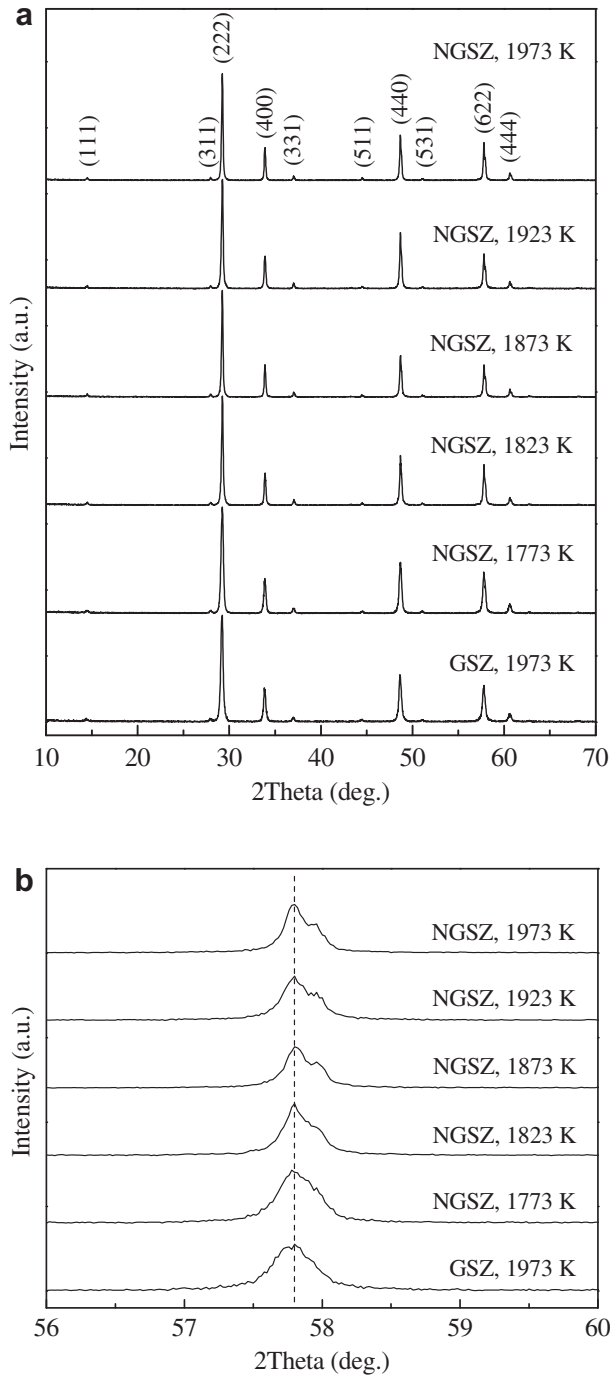

Fig. 1. XRD patterns of the $GdSmZr_2O_7$ ceramic with and without 1 wt.% NiO sintered at different temperatures for 10 h in air: (a) 2θ range of 10–70°, (b) 2θ range of 56–60°.

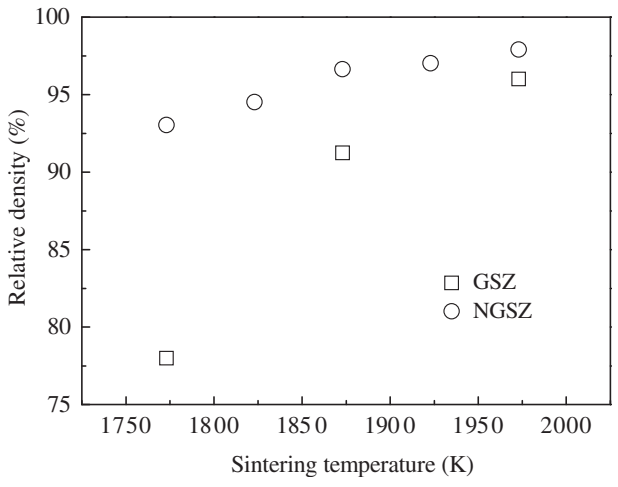

Fig. 2. Relative density of the $GdSmZr_2O_7$ ceramic with and without 1 wt.% NiO sintered at different temperatures for 10 h in air.

emission scanning electron microscope (FEI Quanta 200F, the Netherlands) equipped with energy-dispersive X-ray spectroscopy. The sintered samples were covered with a sputtered thin film of gold to avoid the charging problem and to obtain better image definition.

The electrical conductivity of sintered samples was measured by electrochemical impedance spectroscopy (EIS) in the 40 Hz–4 MHz frequency range using an impedance/gain-phase analyzer (Solartron™ SI 1260, UK). Platinum electrodes were prepared by brush-painting a colloidal platinum paste onto the surface of polished pellets with the dimensions of 8 mm in diameter and 1 mm in thickness. The pellets were then dried and heated at 1223 K for 2 h in air to erase the solvent. Platinum wires were attached to the surface of the pellets for measurements. Measurements were performed in air, with the signal amplitude of 20 mV at open circuit voltage condition using the Zplot software. Data were collected over the temperature range of 773–1173 K in 50 K intervals, with an equilibration time of 30 min before each measurement. The electrical conductivity of sintered samples was also measured at different oxygen partial pressures in a closed tube furnace cell. The oxygen partial pressure $p(O_2)$ ranged from around 1.0×10^{-4} to 1.0 atm, and was monitored by an YSZ sensor. The process involved flushing the system with a N_2–O_2 gas mixture. The impedance data were analyzed using Zview 3.1c software.

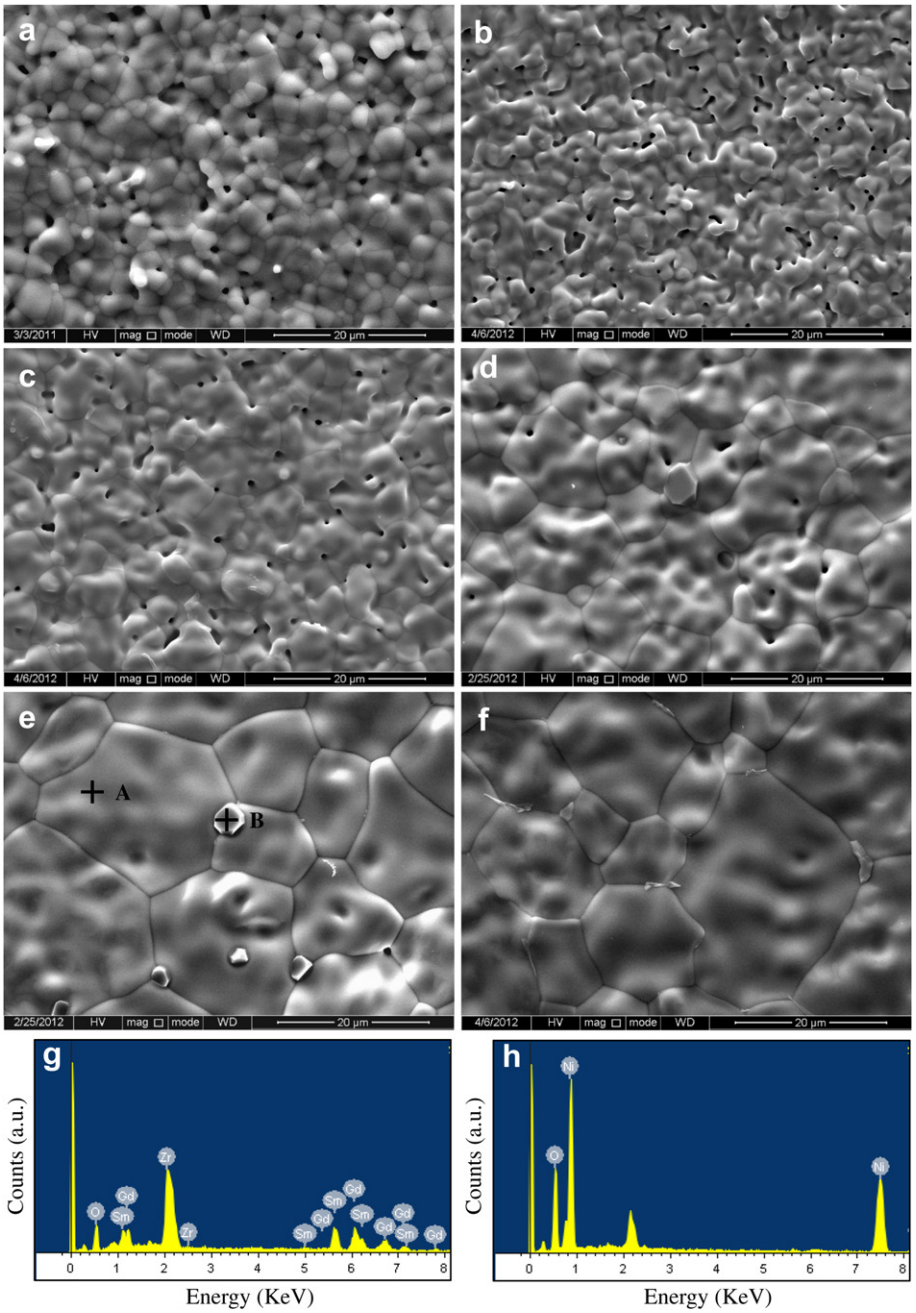

Fig. 3. Surface micrographs and EDX analysis of the $GdSmZr_2O_7$ ceramic with and without 1 wt.% NiO sintered at different temperatures for 10 h in air: (a) GSZ sintered at 1973 K, (b) NGSZ sintered at 1773 K, (c) NGSZ sintered at 1823 K, (d) NGSZ sintered at 1873 K, (e) NGSZ sintered at 1923 K, (f) NGSZ sintered at 1973 K, (g) and (h) EDX spectra at the locations of A and B labeled in (e), respectively.

3. Results and discussion

Fig. 1(a) illustrates the XRD plots of the $GdSmZr_2O_7$ ceramic with and without 1 wt.% NiO sintered at different temperatures for 10 h in air. It can be seen that XRD patterns of the $GdSmZr_2O_7$ ceramic with and without 1 wt.% NiO are very similar, and the diffraction peaks are indexed to (111), (311), (222), (400), (331), (511), (440), (531), (622) and (444) planes, matching well with those of the face-centered cubic pyrochlore-type structure [14,17,21]. No secondary phase could be identified. Fig. 1(b) shows the evolution of the (622) peaks of the $GdSmZr_2O_7$ ceramic with and without 1 wt.% NiO. Clearly, no noticeable peak shift of the (622) except the peak shape change is observed at different sintering temperatures due to the addition of 1 wt.% NiO. From Fig. 1, it is concluded that there is no chemical reaction between $GdSmZr_2O_7$ and NiO, which is consistent with the results reported by Li et al. [22]. Fig. 2 shows the relative densities of the $GdSmZr_2O_7$ ceramic with and without 1 wt.% NiO sintered at different temperatures for 10 h in air. Clearly, the relative densities of the $GdSmZr_2O_7$ ceramic with and without 1 wt.% NiO increase with increasing sintering temperature.

Fig. 3 shows typical micrographs of the $GdSmZr_2O_7$ ceramic with and without 1 wt.% NiO, which are taken from the surfaces of as-sintered samples. As can be seen, the grains of the samples are polygonal, with a heterogeneous distribution. From Fig. 3(a) and (f), the average grain size of the sample NGSZ is obviously larger than that of the sample GSZ sintered at 1973 K. From Fig. 3(b–f), the average grain size of the sample NGSZ gradually increases with increasing sintering temperature. A very small amount of second phase (NiO) can be clearly observed in Fig. 3(d–f), although XRD patterns do not identify the existence of the second phase NiO. The EDS spectra obtained at different positions of A and B labeled in Fig. 3(e) confirm the presence of the $GdSmZr_2O_7$ phase (position A) and NiO phase (position B), as shown in Fig. 3(g) and (h), which are consistent with the above-mentioned XRD results.

Fig. 4 shows the impedance spectra and schematic equivalent electrical circuit plots at 773 K in air corresponding to the $GdSmZr_2O_7$ ceramic with and without 1 wt.% NiO. This temperature of 773 K was chosen for a better comparison of the arcs corresponding to grain resistivity at high frequencies and grain boundary resistivity at intermediate frequencies. It is clearly seen that the sample GSZ exhibits a higher total resistivity than the NiO-modified samples except the sample NGSZ sintered at 1773 K. It is also significant that the sizes of the grain arcs are obviously larger than those of the grain boundary ones. It indicates that the total resistance is mainly governed by the grain resistance. The contributions of grain, grain boundary and electrode–electrolyte are represented by three equivalent circuit units, of which consist parallel resistance and constant phase element (CPE), as shown in Fig. 4(g). Replacing the capacitance by CPE, accounts for the inhomogeneity of microstructure within the sintered samples [23].

The EIS analysis allows separating the grain and the grain boundary contributions to the total impedance. In this work, the contributions from grain and grain boundary were separated at the temperatures lower than 1073 K by analyzing the capacitance of the arcs. The error of grain resistance and grain boundary resistance between the experimental measurements and the fit results from

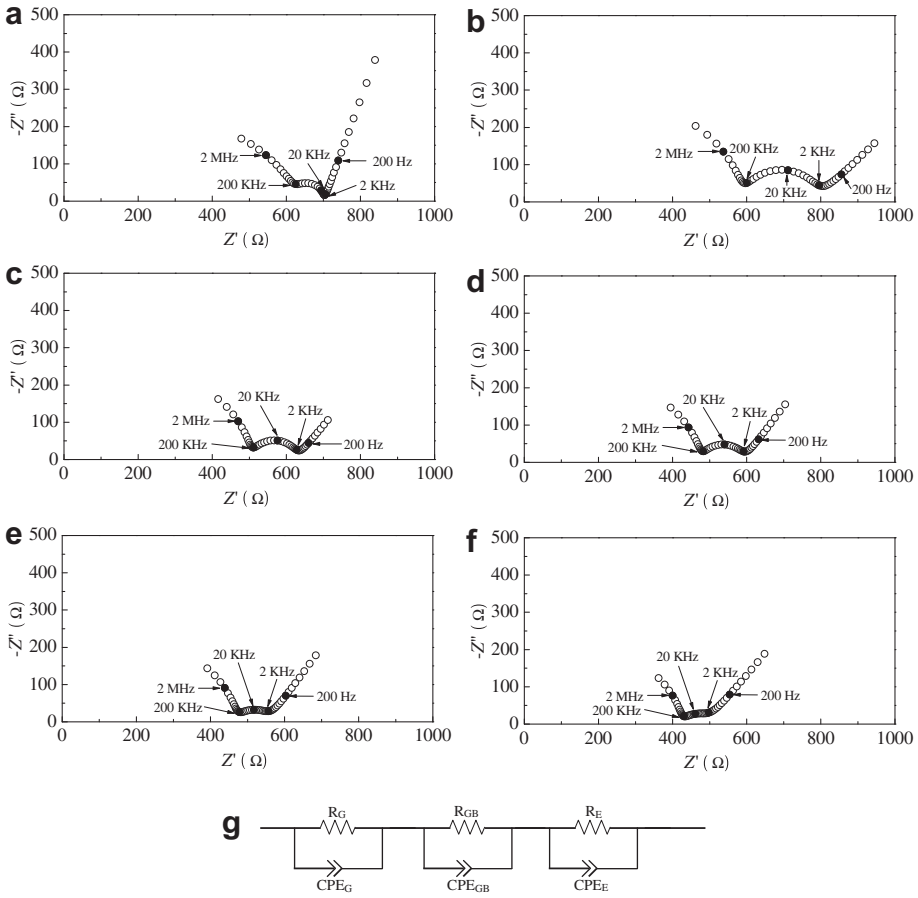

Fig. 4. Impedance spectra and schematic equivalent electrical circuit plots of the $GdSmZr_2O_7$ ceramic with and without 1 wt.% NiO at 773 K in air: (a) GSZ sintered at 1973 K, (b) NGSZ sintered at 1773 K, (c) NGSZ sintered at 1823 K, (d) NGSZ sintered at 1873 K, (e) NGSZ sintered at 1923 K, (f) NGSZ sintered at 1973 K, (g) equivalent electrical circuit.

the equivalent circuit model in Fig. 4(g) using Zview 3.1c is less than 1.0%, respectively. Fig. 5 shows the Arrhenius plots of the grain, the grain boundary, and the total conductivities measured in air. From Fig. 5, the grain conductivities of all measured samples are quite similar, as only very small amount of NiO enters into the grain structure. Compared with the grain conductivity, the grain boundary conductivity exhibits a relatively large change range. This is closely related to the increase in both the grain size and the relative density, and the decrease of the grain boundary density.

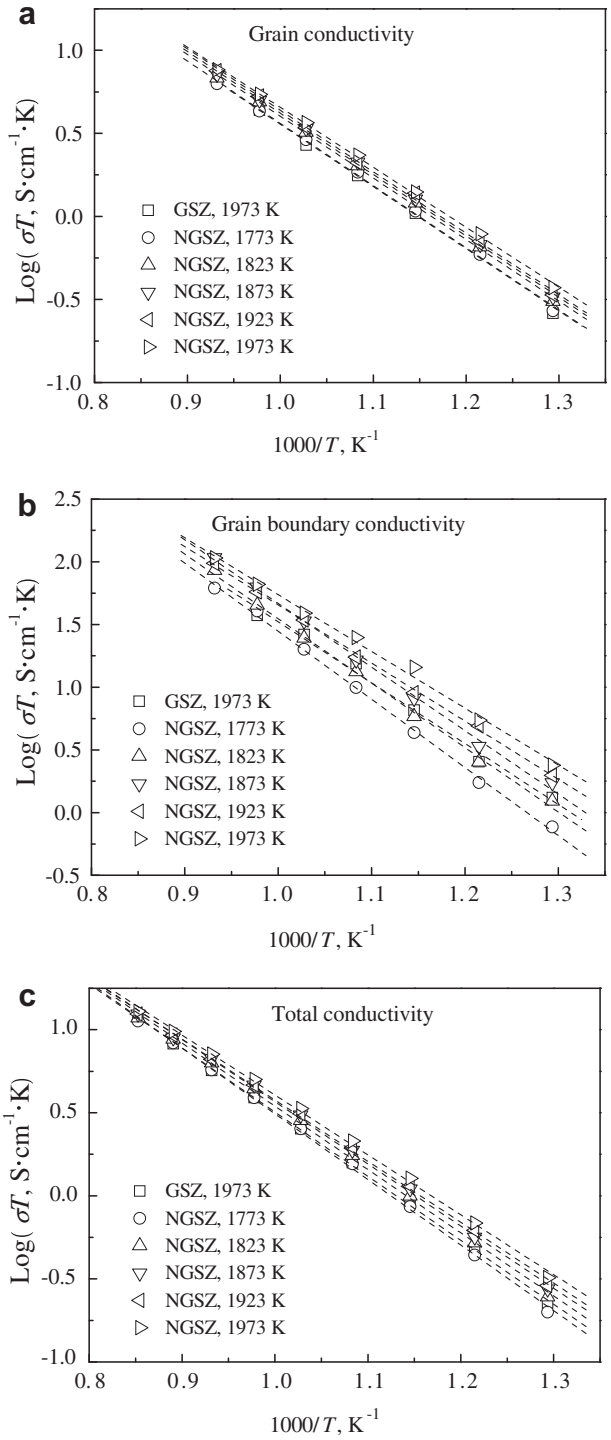

Fig. 5. Arrhenius plots of the $GdSmZr_2O_7$ ceramic with and without 1 wt.% NiO: (a) grain conductivity, (b) grain boundary conductivity, (c) total conductivity.

Table 1
Activation energies of the grain, grain boundary and total conductivity.

Samples	Activation energy (eV)		
	Grain conductivity	Grain boundary conductivity	Total conductivity
GSZ sintered at 1973 K	0.74	0.96	0.77
NGSZ sintered at 1773 K	0.74	1.08	0.78
NGSZ sintered at 1823 K	0.74	1.02	0.76
NGSZ sintered at 1873 K	0.73	1.01	0.74
NGSZ sintered at 1923 K	0.73	0.92	0.73
NGSZ sintered at 1973 K	0.72	0.90	0.72

Table 2
The total conductivities of different sintered samples at typical measurement temperatures.

Samples	773 K ($\times 10^{-4}$ S cm^{-1})	973 K ($\times 10^{-3}$ S cm^{-1})	1173 K ($\times 10^{-2}$ S cm^{-1})
GSZ sintered at 1973 K	2.93	2.60	1.01
NGSZ sintered at 1773 K	2.58	2.60	0.96
NGSZ sintered at 1823 K	3.98	3.30	1.05
NGSZ sintered at 1873 K	3.56	3.16	1.06
NGSZ sintered at 1923 K	3.72	3.21	1.06
NGSZ sintered at 1973 K	5.09	3.44	1.10

The activation energies corresponding to the grain, grain boundary and total conductivities are shown in Table 1. They are in accord with those previously reported in the similar chemical compositions of pyrochlore-type rare-earth zirconates [13,14,16]. The activation energy for the grain conductivity is almost constant, ranging between 0.72 and 0.74 eV, for different sintered samples.

The total conductivities of different sintered samples at typical measurement temperatures are shown in Table 2. Clearly, the total conductivity of the sample NGSZ sintered at 1773 K is comparable to that of the sample GSZ sintered at 1973 K. NiO is an effective sintering aid for the $GdSmZr_2O_7$ ceramic. NiO additive enhances greatly the densification process and the grain growth, and reduces the sintering temperature by about 200 K, without adversely affecting the total conductivity of the $GdSmZr_2O_7$ ceramic. In this work, the total conductivity for the $GdSmZr_2O_7$ ceramic with and without 1 wt.% NiO is about 1×10^{-2} S cm^{-1} at 1173 K in air.

In order to clarify the conduction carrier, the oxygen partial pressure $p(O_2)$ dependence of the total conductivity for the $GdSmZr_2O_7$ ceramic with and without 1 wt.% NiO was measured. Fig. 6 shows the total conductivity of the sample NGSZ sintered at

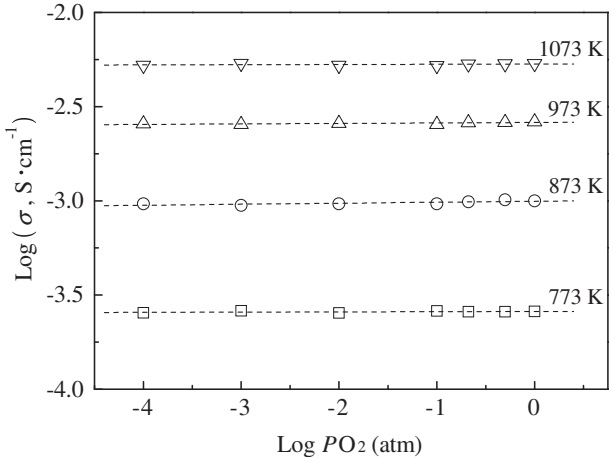

Fig. 6. Oxygen partial pressure dependence of the total conductivity of the sample NGSZ sintered at 1773 K in air.

1773 K as a function of oxygen partial pressure at different temperatures. The total conductivity of the sample NGSZ sintered at 1773 K is almost independent of oxygen partial pressure from 1.0×10^{-4} to 1.0 atm at each test temperature, which indicates that the conduction of the sample NGSZ sintered at 1773 K is purely ionic conductivity with negligible electronic conduction [24]. The total conductivity of conventional solid oxide electrolyte such as $Zr_{0.92}Y_{0.08}O_{2-\delta}$ (YSZ), which is used in SOFCs, is about 8×10^{-2} S cm^{-1} at 1173 K [25]. Taking into account that the total conductivity (about 1×10^{-2} S cm^{-1} at 1173 K) of the $GdSmZr_2O_7$ ceramic with and without 1 wt.% NiO is slightly lower than that of YSZ, the most likely applications of the $GdSmZr_2O_7$ ceramic with and without 1 wt.% NiO in SOFCs are high-temperature solid electrolytes, or thick-film electrolytes, or as protective layers applied onto CeO_2- or $LaGaO_3$-based solid oxide electrolytes [25].

4. Conclusions

The $GdSmZr_2O_7$ ceramic exhibits a single phase of the pyrochlore-type structure. No chemical reaction between $GdSmZr_2O_7$ and NiO is found in the sintered samples. The relative densities of the $GdSmZr_2O_7$ ceramic with and without 1 wt.% NiO increases with increasing sintering temperature. The addition of a small amount of NiO as a sintering aid to the $GdSmZr_2O_7$ ceramic greatly promotes the densification process, achieving 93% of the theoretical density after sintering at 1773 K in air. This reduces the sintering temperature by about 200 K, without adversely affecting the total conductivity of the $GdSmZr_2O_7$ ceramic. The grain, grain boundary, and total conductivity of the $GdSmZr_2O_7$ ceramic with and without 1 wt.% NiO obey the Arrhenius relation. The $GdSmZr_2O_7$ ceramic with 1 wt.% NiO is an oxide-ion conductor in the oxygen partial pressure range of 1.0×10^{-4} to 1.0 atm at all test temperature levels.

Acknowledgments

This work was financially supported by the National Natural Science Foundation of China (NSFC, Grant Nos. 50972030, 51272054 and 51021002), the Fundamental Research Funds for the Central Universities (Grant Nos. HIT.BRET1.2010006 and HIT.NSRIF.201132), the China Postdoctoral Science Foundation funded project (CPSF-Nos. 20100471029 and 201104419), and the Postdoctoral Science Foundation of Heilongjiang Province (LBH–Z10149).

References

[1] L. Malavasi, C.A.J. Fisher, M.S. Islam, Chem. Soc. Rev. 39 (2010) 4370–4387.
[2] E.D. Wachsman, K.T. Lee, Science 334 (2011) 935–939.
[3] A. Aguadero, L. Fawcett, S. Taub, R. Woolley, K.-T. Wu, N. Xu, J.A. Kilner, S.J. Skinner, J. Mater. Sci. 47 (2012) 3925–3948.
[4] W.M. Guo, Y.F. Xiao, X.M. Liu, Y. Chen, L.J. Li, Fuel Cells 11 (2011) 678–681.
[5] K.S. Chang, Y.F. Lin, K.L. Tung, J. Power Sources 196 (2011) 9322–9330.
[6] A. Evans, A. Bieberle-Hutter, L.J. Bonderer, S. Stuckenholz, L.J. Gauckler, J. Power Sources 196 (2011) 10069–10073.
[7] J.A. Díaz-Guillén, A.F. Fuentes, M.R. Díaz-Guillén, J.M. Almanza, J. Santamaría, C. León, J. Power Sources 186 (2009) 349–352.
[8] M. Chen, Y.-L. Liu, A. Hagen, P.V. Hendriksen, F.W. Poulsen, Fuel Cells 9 (2009) 833–840.
[9] M.A. Subramanian, G. Aravamudan, G.V. Subba Rao, Prog. Solid State Chem. 15 (1983) 55–143.
[10] K. Shinozaki, M. Miyauchi, K. Kuroda, O. Sakurai, N. Mizutani, M. Kato, J. Am. Ceram. Soc. 62 (1979) 538–539.
[11] Z.-G. Liu, J.-H. Ouyang, K.-N. Sun, X.-L. Xia, J. Power Sources 195 (2010) 7225–7229.
[12] F.N. Sayed, V. Grover, K. Bhattacharyya, D. Jain, A. Arya, C.G.S. Pillai, A.K. Tyagi, Inorg. Chem. 50 (2011) 2354–2365.
[13] Z.-G. Liu, J.-H. Ouyang, K.-N. Sun, Y. Zhou, Mater. Lett. 65 (2011) 385–387.
[14] Z.-G. Liu, J.-H. Ouyang, Y. Zhou, X.-L. Xia, J. Power Sources 185 (2008) 876–880.
[15] Z.-G. Liu, J.-H. Ouyang, Y. Zhou, J. Li, X.-L. Xia, J. Eur. Ceram. Soc. 29 (2009) 647–652.
[16] X.-L. Xia, J.-H. Ouyang, Z.-G. Liu, J. Am. Ceram. Soc. 93 (2010) 1074–1080.
[17] Z.-G. Liu, J.-H. Ouyang, Y. Zhou, X.-L. Xia, Adv. Appl. Ceram. 109 (2010) 12–17.
[18] R.M. Batista, E.N.S. Muccillo, Ceram. Int. 37 (2011) 1047–1053.
[19] S. Ricote, N. Bonanos, Solid State Ionics 181 (2010) 694–700.
[20] Y. Liu, L. Yang, M.F. Liu, Z.Y. Tang, M.L. Liu, J. Power Sources 196 (2011) 9980–9984.
[21] Z.H. Xu, S.M. He, L.M. He, R.D. Mu, G.H. Huang, X.Q. Cao, J. Alloys Compd. 509 (2011) 4273–4283.
[22] T. Li, S.Z. Zhu, Q. Xu, S. Sun, Z.G. Feng, Rare Met. Mat. Eng. 40 (2011) 615–618.
[23] J.R. Macdonald, W.B. Johnson, in: E. Barsoukov, J.R. Macdonald (Eds.), Impedance Spectroscopy: Theory, Experiment and Applications, second ed., John Wiley & Sons, Inc., New Jersey, 2005 (Chapter 1).
[24] J.B. Goodenough, Annu. Rev. Mater. Res. 33 (2003) 91–128.
[25] V.V. Kharton, F.M.B. Marques, A. Atkinson, Solid State Ionics 174 (2004) 135–149.